RESILIENT INFRASTRUCTURE
June 1–4, 2016
RESILIENT INFRASTRUCTURE LONDON 2016

PUNCHING SHEAR OF SELF-CONSOLIDATING TWO WAY SLABS

Hossameldeen, Bakr
Dillon Consulting Ltd., Canada

Amgad, Hussein
Memorial University of Newfoundland, Canada

Assem, A. Hassan
Memorial University of Newfoundland, Canada

ABSTRACT

This paper presents an experimental program conducted to investigate the punching shear behaviour of self-consolidating (SCC) two-way slabs, and the influence of using different sizes of coarse aggregate and slab thickness on this behaviour. For this purpose, a total of six slabs were tested. Two groups of labs with targeted compressive strength of 30 MPa were used; for group A, 10 mm coarse aggregate size was used, and 20 mm coarse aggregate size was used for the slabs in group B. Each group consisted of three slabs with different thicknesses of 150, 200, and 250 mm. The results revealed a significant effect of slab thickness and size of coarse aggregate. The failure criterion proposed by (Muttoni 2008) based on the slab rotation was used to predict the tested slabs capacities. In addition, comparison with other codes of practice (CSA A23.3-04, ACI 318-11, BS8110-97, and EC2) was carried out. These codes except the EC2 can be safely used to check the punching shear capacity of SCC slabs without the need of any modification to the equations used.

Keywords: punching; aggregate size; self-consolidating concrete

1. INTRODUCTION

Self-consolidating concrete (SCC) was first used in Japan in the 1980s. It is also known as Self-compacting concrete. It was mainly produced to be used in reinforced structures with congested reinforcement (Goodier 2003). SCC has a high ability to flow under its own weight within highly congested reinforced concrete structures without segregation or destruction of mixture homogeneity, and provides good consolidation without need for internal or external compaction (Hassan et al. 2010). The high flowability is the main characteristic of SCC when compared with normal concrete (NC). SCC can be developed by adding superplasticizer to NC mixtures. An SCC mixture has a higher fine aggregate content to improve the flowability and avoid any segregation.

These advantages are the main reasons for the use of SCC as a construction material in applications such as residential and industrial buildings, garages, walls, and bridges. The shear capacity of SCC members could be of concern due to the increased fine aggregate content which is believed to result in a reduction in the shear strength of a structural member. The increased fine content may cause a reduction in aggregate interlock which is considered to be the main resisting factor for shear stresses in beams (Lin et al. 2012). Thus, in the past few years, extensive studies have been conducted on the shear failure mechanism of SCC reinforced beams (Lin et al. 2012) and (Hassan et al. 2008). However, no investigations have been reported on the structural behaviour of SCC reinforced slabs failing due to punching shear stresses. Hence, there is a need to study the punching shear strength of SCC two-way slabs. Punching shear is a brittle mode of failure which occurs without warning.

A rational mechanical model was proposed by (Muttoni 2008) and subsequently formed the basis of the punching shear provisions in the latest edition of the Model Code (2010). The model includes the effect of the coarse aggregate size to predict the behaviour and capacity of the two-way slabs based on the load-rotation relationship.

No other rational model or code equation accounts for the coarse aggregate size effect on the behaviour and capacity of the two-way slab. From the literature, the model gives good predictions for the NC slabs. On the other hand, the provisions of the design codes (CSA 23.3-04, ACI 318-11, BS 8110-97, and EC2) for punching shear are based on empirical formulas. These formulas were developed based on research conducted on NC slabs. Thus, it is necessary to examine the application of the code equations in the design of SCC slabs for punching shear.

The current study was conducted to investigate the influence of changing the coarse aggregate size and slab depth on the behaviour and capacity of SCC slabs. The results were used to investigate the adequacy of the current codes of practice and Muttoni's failure criterion to predict the punching capacity of two-way SCC slabs.

2. EXPERIMENTAL PROGRAM

2.1 Materials and Mixture Design

Two different concrete mixtures were used in the current experimental work. The mixtures were supplied from a local batch plant and were designed to achieve a compressive strength of 30 MPa after 28 days. Details of the mixtures are given in Table 1. Two different coarse aggregate sizes were used; namely 10 and 20 mm. Type GU Portland cement and Class F fly ash (ASTM Type I) were used as binder. The coarse and fine aggregates were crushed granite. A high range water reducing agent (HRWRA) was used to achieve the required slump flow diameter of 650 ± 50 mm for both mixtures. The chemical admixture was added to the mixture after the concrete truck arrived at the structures lab.

Table 1: Mixture Proportions for the SCC Chosen Mixtures

Mixture No.	Total Binder (kg/m^3)	Cement (kg/m^3)	Fly Ash %	Fly Ash (kg/m^3)	CA Size (mm)	C/F	CA (kg/m^3)	FA (kg/m^3)	W/B	Water (L/m^3)	HRWRA (L/m^3)
Mix A	500	200	60	300	10	1.2	865	721	1.0	200	0.78
Mix B	500	200	60	300	20	1.2	865	721	1.0	200	1.10

CA: coarse aggregate; FA: fine aggregate; C/F: coarse to fine aggregate ratio; W/B: water to total binder ratio, and HRWRA: high range water reducing agent.

2.2 Fresh and Hardened Properties Tests

The fresh properties tests (slump flow, V-Funnel, and L-Box) were carried out to ensure that both mixtures satisfy the SCC requirements. The slump flow and V-Funnel tests were conducted to investigate the mixture flowability and viscosity by measuring the slump diameter and T_{500} for the slump flow test, and initial time (t_0) for the V-Funnel test. The L-Box was performed to investigate the passing ability. They were performed according to The European Guidelines for Self-Compacting Concrete (2005) and the results are listed below in Table 2.

Table 2: Fresh Properties for the SCC Chosen Mixtures

Mixture No.	Compressive Strength (MPa)	Flexure Strength (MPa)	Slump Flow (mm)	T_{500} (sec)	H2/H1 L-Box	Initial V-Funnel (sec)	HRWRA (L/m^3)
Mix A	30.0	3.64	650	1.4	0.55 (0.83)	2.7	0.78
Mix B	24.5	3.47	630	3.0	0.73	9.0	1.10

The flexure strengths were obtained according to ASTM C78 using 100 × 100 × 400 mm prism. The flexure strength listed in Table 2 is the average value of four prisms tested after 28 days of casting. The compressive strength was obtained in accordance with ASTM C39-04 using 100 mm diameter × 200 mm cylinders. The compressive strength value listed in Table 2 is the average value of three cylinders tested at the same day of testing the slab.

2.3 Test Slabs

Figure 1 shows the details of a typical test slab. All slabs had side dimensions of 1900 mm × 1900 mm. A total of six slabs were tested. Table 3 lists the details of the test slabs. The main variables were the maximum coarse aggregate size and slab thickness. Two maximum coarse aggregate sizes of 10 and 20 mm, and three slab thicknesses of 150 mm, 200 mm, and 250 mm were used. The concrete cover was 25 mm. The target reinforcement ratio was 1% and it slightly varied for the slabs with different thicknesses to maintain the same spacing between the reinforcement. The flexural reinforcement ratios were 1.01%, 1.08%, and 0.91% for the slabs with thicknesses of 150, 200, and 250 mm, respectively.

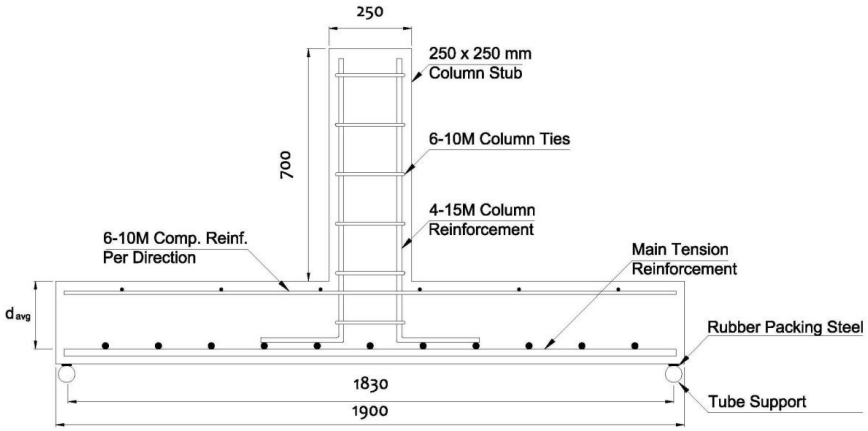

Figure 1: Typical Test Slab Details

Table 3: Details of Test Slabs

Slab No.	Compressive Strength (MPa)	CA Size (mm)	Bar size (mm)	Bar spacing (mm)	Concrete cover (mm)	Slab thickness (mm)	Slab depth (mm)	Flexure reinforcement ratio ρ, %
SCA150	29.0	10	15M	180	25	150	110	1.01
SCA200	30.0	10	20M	180	25	200	155	1.08
SCA250	32.0	10	20M	160	25	250	205	0.91
SCB150	24.0	20	15M	180	25	150	110	1.01
SCB200	24.5	20	20M	180	25	200	155	1.08
SCB250	25.0	20	20M	160	25	250	205	0.91

*SC is self-consolidating slabs; A/B is mixture number, followed by the slab thickness

2.3 Test Setup

A steel frame, located in the structures lab at Memorial University of Newfoundland was used for testing all slabs (Figure 2). The slabs were simply supported on all four sides. The simply supported edges simulate the lines of contra-flexure, and hence, the test slabs represent the region of negative bending moment around an interior column. The four edges of the test slab were supported on 32 mm diameter rods covered with 3.0 mm layer of rubber strips placed along the contact line between the rods and the slabs to minimize the resulted friction. A hydraulic actuator with maximum capacity of 1783 kN was fixed to the frame and used to apply the concentric loaded through a 250 × 250 mm square column stub. The applied load and the displacement were measured using a pressure transducer and a linear voltage displacement transducer (LVDT), respectively.

Figure 2: Test Setup: (a) Testing Frame Front View; (b) Data Acquisition System and Testing Frame Layout

2.3 Instrumentation Test Procedure

Four linear variable differential transducers (LVDTs) were located at the tension side of the slab, as shown in Figure 3(a). Their results were used to plot the load-deflection curves and deflection profiles. The reinforcement strains were monitored at ten locations, as shown in Figure 3(b). The strains were measured using electrical strain gauges with gauge factor 2.075 ± 0.5% and resistance of 120 ± 0.30% Ω at 24℃. The strain gauge locations were selected to detect the strains in the flexural reinforcement and the strain variation in both the radial and tangential directions.

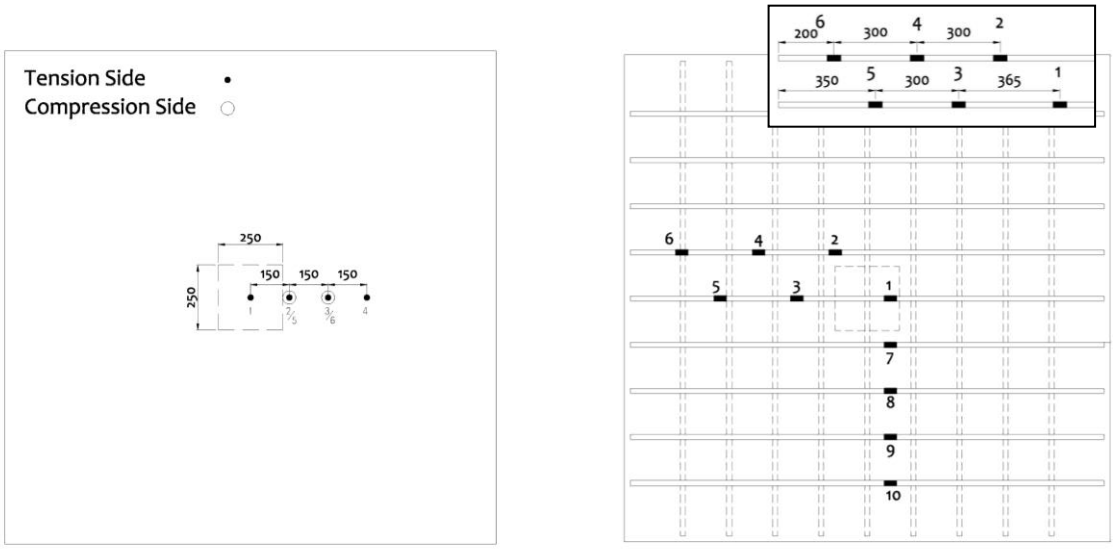

Figure 3: Test Setup: (a) LVDTs Arrangement; (b) Steel Strain Gauges Arrangement

The data collected from the strain gauges and LVDTs were logged to a high speed data acquisition system using LAB-View software and stored on a personal computer.

The slabs were placed in a vertical position. Their position was adjusted to ensure that the column stub center coincides with the loading actuator axis. At the beginning of the test, an initial load was applied to the slab to ensure that all the four sides were rested on the rods and the initial settlement was reduced. The load was applied at a load increment of 8.8 kN (2.0 kips) until the first crack was detected. The test was then resumed using load increments of 22.5 kN (5 kips). At each load step the test was stopped and the crack propagation was marked.

3. TEST RESULTS

3.1 Load-deflection Characteristics

Figure 4 shows the applied load versus the central deflection of all test slabs. The small initial settlement in the load-deflection graphs was corrected. Table 4 shows the load and the corresponding deflection values at first crack, first yield of the flexure reinforcement, and at ultimate load. The first crack was observed by the naked eye. However, a reliable value for the first crack could not be observed by the naked eye for slabs SCA250 and SCB200 ; the crack appeared at the surface at unreasonably high values. The load that corresponds to the first yielding of the flexure reinforcement was determined from the strain gauges' readings. Some strain gauges malfunctioned and the readings could not be recorded. The first yielding of the flexural reinforcement is indicated by a circle on each curve where possible. This figure was plotted in order to examine the effect of changing the slab thickness as well as changing the maximum aggregate size from 10 mm to 20 mm. It was found that using larger maximum coarse aggregate size of 20 mm, resulted in higher capacities and lower deflection values compared to those resulted in slabs of mixture A where maximum coarse aggregate size of 10 mm was used.

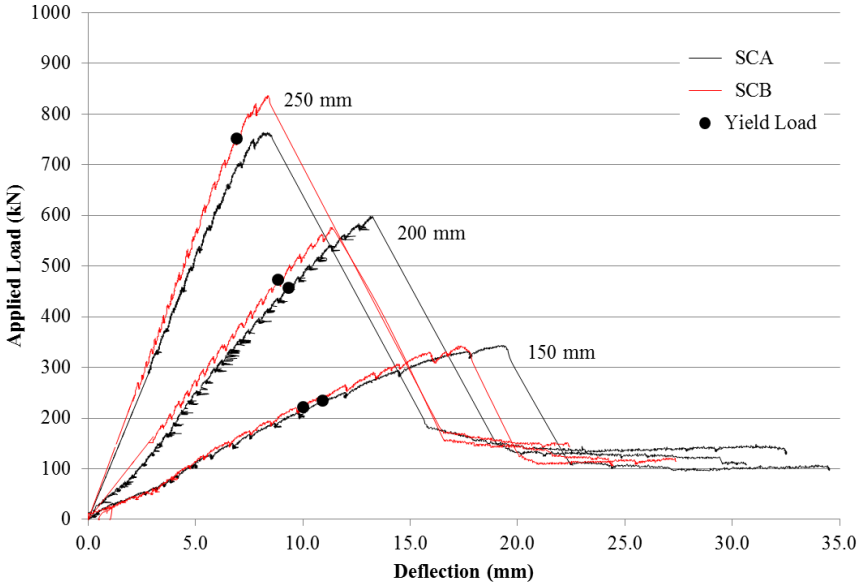

Figure 4: Load-deflection Characteristics at Slabs Center

Table 4: Deflection Characteristics of Test Slabs

Slab No.	Compressive strength (MPa)	Aggregate size (mm)	First crack load (kN)	First crack deflection (mm)	Yield load (kN)	Yield load deflection (mm)	Ultimate load (kN)	Ultimate load deflection (mm)
SCA150	29.0	10	55	2.70	234	10.90	343	19.30
SCA200	30.0	10	62	1.40	457	9.30	598	13.20
SCA250	32.0	10	-	-	-	-	764	8.35
SCB150	24.0	20	45	2.30	221	10.0	342	17.40
SCB200	24.5	20	-	-	473	8.80	576	11.40
SCB250	25.0	20	100	0.90	751	6.90	836	8.40

The deflection values listed in Table 4 illustrate a significant effect of changing the slab thickness. The deflection at ultimate load for the 250 mm thick slabs was 50% of that of the 150 mm thick slabs. This can be attributed to the increase in stiffness resulted from increasing the slab thickness. The thin slabs showed more ductile failure behaviour as they exhibited higher deflection values. The 150 mm thick slabs failed in ductile punching shear. However, thicker slabs (200 mm and 250 mm) failed due to pure punching shear.

3.2 Flexure Reinforcement Strain

Figure 5 shows a typical plot of the applied load versus strain in the flexure reinforcement at the center of each slab. The highest strains in the flexural reinforcement were observed at that location. Higher strain values were recorded in the thinner slabs. This finding was confirmed from the readings of the ten strain gauges used. Yielding of flexural reinforcement was more spread in the 150 mm thick slabs and localized around the column stub in the 200 mm and 250 mm thick slabs. None of the tested slabs reached the flexure failure load according to the yield line theory. The figures also show a slight change in the slope of the load-strain curves. This change approximately corresponds to where the first crack was formed on the slab surface.

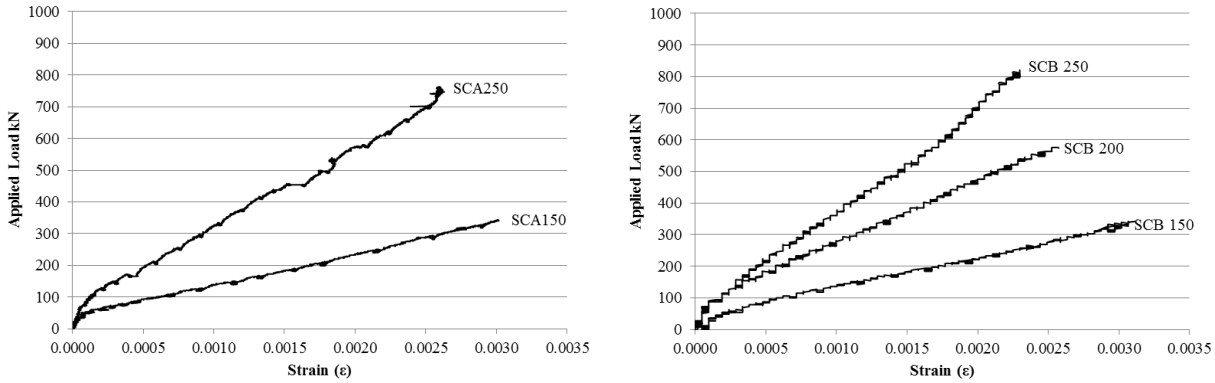

Figure 5: Load versus Reinforcement Strains at the Centre of the Slabs

3.3 Shear Strength

The shear strengths for all slabs are presented in this section. The recorded ultimate loads, P_{test}, are listed in Table 5. The shear strength, v_u, is determined by dividing the ultimate load by $b_o d$, where b_o is the critical punching perimeter at d/2 from the column face, and d is the average slab depth for punching shear stresses calculations. In order to eliminate the small variability in the compressive strength of the different slabs, the shear strength was normalized by dividing v_u by the square root of the compressive strength.

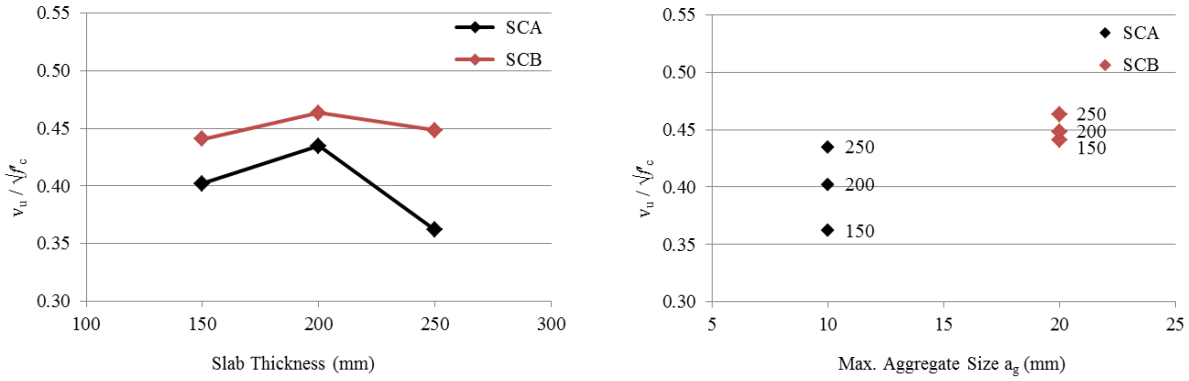

Figure 6: Shear Stresses: (a) Stresses versus Slab Thickness; (b) Stresses versus Maximum Coarse Aggregate Size

The relationship between the normalized shear strength and the slab depth is shown in Figure 6(a) for all test slabs. The 200 mm and 250 mm thick slabs in Group A and B indicated a decreasing trend in the normalized shear strength with increasing slab depth. However, SCA150 and SCB150 did not show the same trend of decreased normalized shear strength when the slab depth is increased.

Figure 6(b) shows the normalized shear strength versus the aggregate size for all test slabs. The figure clearly demonstrate that the coarse aggregate size have a significant influence on the shear strength of the test slabs. The shear strength consistently increased with increasing the maximum coarse aggregate size as listed in Table 5.

3.4 Slab Rotation and Ultimate Capacity

A rational mechanical model was proposed by (Muttoni 2008) and subsequently formed the basis of the punching shear provisions in the latest edition of the Model Code (2010). The proposed failure criterion relates the punching shear strength of the two-way slab with the slab rotation. It is assumed that the shear strength is governed by the width and the roughness of the shear crack developed through an inclined compression strut that carries the shear force; assuming that the crack width is proportional to the slab rotation. The shear strength is calculated from a set of assumed kinematics characterized by the rotation of the slab and integrating the contribution of the concrete tensile stresses, and the aggregate interlock along the failure surface. Most of the shear stress is transferred at the bottom end of the crack where the crack width is small, while any contribution from dowel action of the reinforcement is ignored due to the expected spalling of the concrete cover. It should be noted that the CSCT failure criterion despite the other codes used, takes into account both the slab rotation and the maximum coarse aggregate size. In this study, the resulted ultimate loads were compared with those predicted by the new failure criterion.

In Figure 7, the CSCT failure criterion for the current test slabs is represented by the dashed lines calculated using Eq. 1, where ψ is the slab rotation, d_g is the maximum aggregate size, and d_{g_0} is a reference size equal to 16 mm.

$$[1] \quad \frac{V_R}{b_0 d\sqrt{f_c'}} = \frac{3/4}{1+15\dfrac{\psi d}{d_{g_0}+d_g}}$$

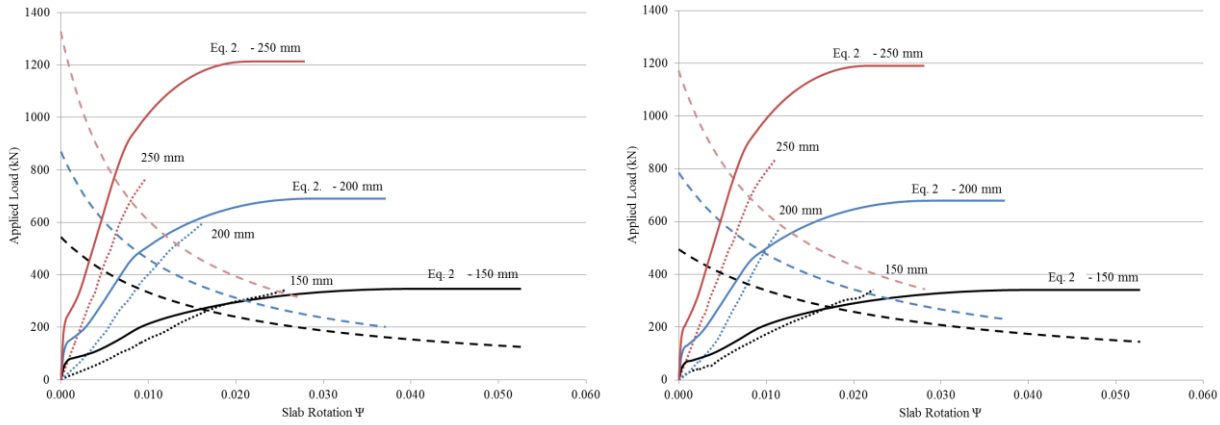

Figure 7: Load versus Slab Rotation of Test Slabs: (a) Slabs of Mixture A, and (b) Slabs of Mixture B

The solid lines represent the slab-rotation of the current test slabs as predicted using Eq. 2. The applied load versus rotation obtained from the experimental work for each slab is represented by the dotted curves on those figures.

$$[2] \quad V = \frac{2\pi}{r_q - r_c}\left(-m_r r_0 + m_R\langle r_y - r_0\rangle + EI_1\psi\langle \ln(r_1) - \ln(r_y)\rangle + EI_1\chi_{TS}\langle r_1 - r_y\rangle + m_{cr}\langle r_{cr} - r_1\rangle + EI_0\psi\langle \ln(r_s) - \ln(r_{cr})\rangle\right)$$

The capacity and corresponding maximum rotation predicted using the CSCT failure criterion are defined by the intersection of the slab-rotation curve (solid line) with the failure criterion (dashed line). The measured ultimate loads and rotations as well as those predicted using CSCT are listed in Table 5. The slab rotations at ultimate loads are also listed in Table 5 for all test slabs. These rotations were measured for the slab portion outside the shear crack which rotates as a rigid body.

The experimental results confirm the major influence of the slab thickness on the rotation capacity. Thick slabs were found to have lower rotation capacity compared to thin slabs. No significant is found due to changing the coarse aggregate size. Figure 7 and Table 5 reveal that the CSCT reasonably predicts the load-rotation behaviour of all test slabs. However, the initial stiffness is overestimated by the CSCT. This overestimation is more pronounced for slabs with thicknesses of 200 and 250 mm.

Table 5: Test Results versus CSCT Predictions

Slab No.	Compressive Strength (MPa)	P_{test}	P_{CSCT}	Experimental Rotation	CSCT Rotation	P_{CSCT}/P_{test}	$v_u / \sqrt{f_c'}$
SCA150	29.0	343	276	0.0256	0.0153	0.80	0.402
SCA200	30.0	598	490	0.0162	0.0087	0.82	0.435
SCA250	32.0	764	770	0.0096	0.0061	1.01	0.362
SCB150	24.0	342	282	0.0223	0.0166	0.82	0.441
SCB200	24.5	576	493	0.0115	0.0092	0.86	0.463
SCB250	25.0	836	763	0.0110	0.0063	0.91	0.448

3.5 Test results versus code predictions

In this study, the test results were compared to the predictions of CSA A23.3-04, ACI 318-11, BS8110-97, and EC2-2010 design codes. When calculating the shear stresses, the control perimeter is considered at different distances from the column face. In the CSA A23.3-04 and ACI 318-11 it is located 0.50d from the column face, and in BS8110-97, and EC2-2010. It is 1.5d and 2.0d, respectively. CSA A23.3-04 does not account for the coarse aggregate size or the slab depth if it is less than 300 mm. However, BS8110-97, and EC2, 2010 contains terms that account for the slab depth. It should be mentioned that the BS 8110 code was superseded by Eurocode (EC2) in 2010. The resistance factors in these equations are taken as unity when comparing the predication of the code equations to the test results

Table 6: Test Results versus Codes Predictions

Slab No.	Compressive Strength	Ultimate load, P_{test}	Nominal shear stress*	P_{test}/P_{code}				P_{test}/P_{flex}
	(MPa)	(kN)		CSA23.3	ACI318	BS8110	EC2	
SCA150	29.0	343	0.402	0.94	0.82	0.94	0.98	0.75
SCA200	30.0	598	0.435	0.87	0.76	0.88	1.04	0.64
SCA250	32.0	764	0.362	1.05	0.91	0.99	1.26	0.56
SCB150	24.0	342	0.441	0.86	0.75	0.88	0.92	0.77
SCB200	24.5	576	0.463	0.82	0.71	0.85	1.00	0.63
SCB250	25.0	836	0.448	0.85	0.74	0.83	1.06	0.63

* $v_u = P_{test} / b_0 d\sqrt{f_c'}$

In the CSA A23.3-04, the ultimate shear resistance for the two-way slabs is equal to the smallest if the following equations;

[3] $$v_c = \left(1 + \frac{2}{\beta_c}\right) 0.19 \lambda \phi_c \sqrt{f_c'}$$

[4] $$v_c = \left(\frac{\alpha_s d}{b_0} + 0.19\right) \lambda \phi_c \sqrt{f_c'}$$

[5] $$v_c = 0.38 \lambda \phi_c \sqrt{f_c'}$$

where β is the ratio of long side to short side of the column, λ is the concrete density factor, ϕ_c is the resistance factor for concrete, and α_s is adjusting factor (α_s = 4 for interior columns, 3 for edge columns, and 2 for corner columns).

A comparison between the resulted ultimate loads and the different codes predications is presented in Tables 6. The ACI 318-11 gives the most conservative predictions for the ultimate loads. The CSA A23.3-04 gives safe predictions for all slabs except slab SCB250. Hence, the CSA code is more conservative and has less scatter for SCC slabs with 20 mm coarse aggregate size compared to those with 10 mm coarse aggregate size. The BS8110-97 gives safe predictions and the least scatter of the P_{code}/P_{test} ratios for slabs with 10 mm coarse aggregate size. The BS8110-97 results were very similar to those of CSA A23.3 for the slabs of 20 mm coarse aggregate size. The EC2-2010 predictions are unsafe for the slabs with thicknesses of 200 mm and 250 mm.

4. CONCLUSION

In this study, two SCC mixtures were developed. Six reinforced slabs were prepared using these developed mixtures to investigate the influence of using different maximum coarse aggregate size and slab depth. The fresh and hardened properties were tested. The structural behaviour and characteristics of the slabs were examined (load-deflection, flexure reinforcement strain, and the ultimate capacities. The following conclusions can be drawn from the results of this study:

1. The slab thickness has the most significant effect on the behaviour of the test slabs.
2. The depth and aggregate size are the most influential parameters on the shear capacity of the slab; increasing the slab thickness lead to a decrease in the normalized shear strength of the slab while increasing the aggregate size lead to an increase in the normalized shear strength of the slab.
3. The punching shear provisions in the Model Code (2010) are based on the CSCT proposed by Muttoni (2008). The CSCT is able to reasonably predict the structural behaviour of the test slabs. Nonetheless, the test results did not show any clear trend in the relationship between the aggregate size and the slab rotation.
4. The CSA A23.3-04, ACI 318-11 and BS8110-97 give safe predictions of the SCC test slabs capacities. The only unsafe prediction by CSA A23.3-04 is that for slab SCB250. Therefore, these codes can be safely used to check the punching shear capacity of SCC slabs without the need of any modification to the equations used for such shear check.
5. The predictions of the CSA A23.3-04, ACI 318-11 and BS8110-97 are more conservative and have less scatter when applied to SCC slabs with 20 mm coarse aggregate size compared to those with 10 mm coarse aggregate size.
6. The BS8110-97 was superseded by Eurocode (EC2) in 2010. The predictions of the Eurocode (EC2) are unsafe for most of the slabs with thicknesses of 200 mm and 250 mm.
7. The CSCT gives safe predictions of the capacity all test slabs.

ACKNOWLEDGEMENT

The authors are thankful to the technical staff at the Structural Laboratory of Memorial University of Newfoundland for their continuous support and assistance in preparing the testing samples and during testing. Sincere thanks are extended to Capital Ready Mix Ltd., Newfoundland, Canada for providing the testing materials, and Dillon Consulting Ltd., Windsor, Canada, for providing technical and financial support.

REFERENCES

ACI Committee 318. 2008. Building Code Requirements for Structural Concrete (ACI 318-11) and Commentary, American Concrete Institute, Farmington Hills, MI, USA.

ASTM C39/C39M-04a. 2004. Standard Test Method for Compressive Strength of Cylindrical Concrete Specimens. ASTM International, West Conshohocken, PA. USA.

ASTM C78-02. 2002. Standard Test Method for Flexural Strength of Concrete (Using Simple Beam with Third-Point Loading. ASTM International, West Conshohocken, PA, USA.

Birkle, G., and Dilger, W. 2008. Influence of Slab Thickness on Punching Shear Strength. ACI Structural Journal, 105 (2): 180-188.

BS 8110. 1997. Structural Use of Concrete, Part 1: Code of Practice for Design and Construction. British Standards Institution, London, UK.

BS EN 1992-1-2. 2004. Eurocode 2: Design of Concrete Structures—Part 1-1: General Rules and Rules for Buildings. Brussels, Belgium.

CSA A23.3-04. 2004. Design of Concrete Structures for Buildings. Canadian Standards Association, Rexdale, ON, Canada.

EFNARC. 2005. Specification and Guidelines for Self-Compacting Concrete. Association House, Farhjam, Surrey, UK.

Goodier, C.I. 2003. Development of self-compacting concrete. Structures & Buildings, 156 (SB4): 405-414

Guandalini, S., Burdet, O. L., and Muttoni, A. 2009. Punching Tests of Slabs with Low Reinforcement Ratios. ACI Structural Journal, 106 (1): 87-85.

Hassan, A. A. A., Hossain, K. M. A., and Lachemi, M. 2008. Behaviour of full-scale Self-consolidating concrete beams in shear. Cement & Concrete Composites, 30 (2008): 588-596.

Hassan, A. A. A., Hossain, K. M. A., and Lachemi, M. 2010. Strength, cracking and deflection performance of large-scale self-consolidating concrete beams subjected to shear failure. Engineering Structures, 32 (2010): 1262-1271

Lin, C. H., and Chen, J. H. 2012. Shear Behaviour of Self-consolidating concrete Beams. ACI Structural Journal, 109 (3): 307-316.

Muttoni, A. 2008. Punching shear strength of reinforced concrete slabs without transverse reinforcement. ACI Structural Journal. 105: 440–450.

Rizk, E., Marzouk, H., and Hussein, A. 2011. Punching Shear of Thick Plates with and without Shear Reinforcement. ACI Structural Journal. 108 (5): 581-591.